

Article

# Research on Yaw Stability Control Strategy Based on Direct Slip Rate Allocation

Jing Li \*, Jin Luo , Shiyao Guo and Baidong Feng

School of Vehicles and Energy, Yanshan University, Qinhuangdao 066004, China;

luojin01@stumail.ysu.edu.cn (J.L.); guoshiyao@stumail.ysu.edu.cn (S.G.); bdfeng@stumail.ysu.edu.cn (B.F.)

\* Correspondence: lij@ysu.edu.cn

**Abstract:** This paper deals with the integrated control of trajectory tracking and yaw stability for autonomous vehicles. Firstly, a nonlinear vehicle dynamics model is established. The MPC algorithm was used to determine the best front wheel angle. The PID control algorithm is used to ensure the accuracy of longitudinal speed tracking. The sliding mode control algorithm is used to generate additional yaw moment and optimize the distribution of longitudinal tire force. In order to ensure the most effective distribution of the driving torque of the four wheels of the vehicle, the PID algorithm is used to track and manage the longitudinal slip rate of each tire on the bottom layer. Simulation tools such as MATLAB/Simulink and Carsim are used to verify the effectiveness of the multi-closed-loop integrated control technology. Compared with the general control strategy (no slip rate control), the trajectory error of this control algorithm is reduced by 55.6%, which indicates that it has advantages in obtaining a high tracking accuracy and ensuring the stability of autonomous vehicles.

**Keywords:** trajectory tracking; stability control; integrated control; tire sliding rate control; MPC



**Citation:** Li, J.; Luo, J.; Guo, S.; Feng, B. Research on Yaw Stability Control Strategy Based on Direct Slip Rate Allocation. *Electronics* **2024**, *13*, 193. <https://doi.org/10.3390/electronics13010193>

Academic Editors: Felipe Jiménez and Mahmut Reyhanoglu

Received: 29 November 2023

Revised: 14 December 2023

Accepted: 29 December 2023

Published: 1 January 2024



**Copyright:** © 2024 by the authors. Licensee MDPI, Basel, Switzerland. This article is an open access article distributed under the terms and conditions of the Creative Commons Attribution (CC BY) license (<https://creativecommons.org/licenses/by/4.0/>).

## 1. Introduction

The advent of autonomous driving technology has introduced novel opportunities and challenges arising from the development of intelligent and electric technologies. It has great potential to enhance traffic safety and mitigate environmental pollution. The implementation of distributed-drive four-wheel hub electric cars, equipped with four hub motors that can individually modulate the torque of each wheel, can significantly enhance vehicle mobility and steering precision. A crucial component of autonomous vehicle technology is precise trajectory tracking control. Research on trajectory tracking and vehicle stability management in complex operational environments continues to be a prominent area of investigation in the field of autonomous vehicles.

To address this issue, a range of trajectory tracking control methods have been proposed by scholars. These include pure tracking algorithms, feedforward–feedback control, preview tracking optimal control, linear quadratic regulator (LQR) tracking control, and model predictive control (MPC). Pure tracking algorithms are effective for vehicle tracking at medium and low speeds [1,2]. Feedforward–feedback tracking control relies on the real-time calculation of future road curvature and state feedback to ensure stable driving and trajectory tracking [3]. Preview tracking optimal control uses a driver’s preview optimal curvature model to achieve trajectory tracking [4,5], but requires the constant adjustment of control parameters due to its weak adaptability. LQR tracking control establishes an accurate linear model for trajectory tracking control [6,7], but struggles with nonlinear trajectory tracking in the presence of significant road curvature and external interference. The MPC control algorithm, however, achieves optimal control of trajectory tracking through the rolling optimization of control inputs and feedback correction via a future state prediction of the system, showing strong robustness [8,9].

Model Predictive Control (MPC) is a control method that utilizes a predictive model, rolling optimization, and feedback correction to form a closed-loop control for the entire

algorithm. It is particularly suitable for controlling models with a low accuracy and nonlinearity and can ensure the maximum stability of the controller. As a result, MPC has been extensively applied when tracing the trajectory and controlling stability of autonomous vehicles [10]. With the ongoing development of MPC, researchers have proposed various control algorithms based on the MPC algorithm for vehicle dynamics' control. For instance, Wang et al. [11] proposed using fuzzy control to optimize the weighting matrix of the objective function and applied the improved MPC algorithm to enhance the trajectory tracking and stability of autonomous driving. Sun et al. [12] proposed an adaptive model predictive control algorithm and designed a steering angle monitor to obtain the vehicle's steering angle, thus achieving a means of vehicle trajectory tracking and stability control. A linear model predictive control algorithm (LMPC) with a multi-layer control system has been proposed in [13,14]. Zhang et al. [15] designed a multi-objective model predictive extension coordinated control strategy to achieve vehicle trajectory tracking and lateral stability at high speed. KABZAN J et al. [16] developed a model prediction controller driven by online learning data to ensure vehicle safety while achieving the stable tracking of vehicle trajectories. ROSOLIA U et al. [17] established an optimal decision model for vehicle trajectory tracking using a stochastic MPC control. LEMANZ A et al. [18] used the MPC control algorithm to carry out an obstacle avoidance path tracking control of vehicles at high speed and achieved a better trajectory tracking ability compared to the Stanley controller. These studies demonstrate the effectiveness and versatility of MPC for autonomous vehicle control.

The above paper creates many control algorithms for intelligent vehicle trajectory tracking. However, the problem of yaw stability occurs when the vehicle runs at high speeds and with low road adhesion, which leads to low track tracking accuracy and instability in the vehicle. Therefore, many researchers studied the integrated control of vehicle trajectory tracking and yaw stability. In this paper [19], a force-driven switching MPC path tracking control strategy, with front-wheel active steering and external yaw torque, is proposed. The control strategy can improve the control precision and ensure the stability of the vehicle. In this paper [20], a comprehensive control framework for lateral stability and trajectory tracking, considering the steering force loss caused by combined slip effects, is proposed. Real-time experiments and simulations show that the proposed control framework is superior to existing algorithms in dealing with the problem of reduced tire capacity in rough maneuvers due to simultaneous vehicle and wheel stabilization and path tracking. In this paper [21], a vehicle stability control hardware-in-the-loop test bench was studied, aiming to reduce the experimental cost and provide a new experimental defense. The path tracking integrated control of vehicles with four-wheel independent drive has been explored in the literature [22,23], revealing that integrating or layering the drive torque vector control and front-wheel steering control significantly enhances the precision and stability when tracking the vehicle's path. Other studies [24–29] have also investigated stability control, with approaches including simultaneously distributing left and right wheel torque based on their strength, vertical load, and glide rate control, establishing a two-layer learning MPC control, proposing a new braking torque distribution method using a nonlinear slip rate model, and designing a slip energy and stability control framework to control the transverse and longitudinal dynamics of the vehicle. Reference [30] proposes an integrated control strategy based on the MPC framework, which realizes the trajectory tracking and stability control of the vehicle at high speed.

To summarize, previous studies have made significant progress in the trajectory tracking of autonomous vehicles driven by four-wheel hubs. On the basis of the above research, this paper puts forward a strategy and method for vehicle trajectory tracking and yaw stability control based on the new direct slip rate control method. This paper aims to realize the path-following control and vehicle-dynamic control of high-speed electric vehicles independently driven by intelligent four-wheel motors through a hierarchical control strategy and multiple control algorithms.

In summary, the main contributions of this paper are as follows:

- (1) This paper proposes a three-layer integrated control framework. In the track tracking layer, MPC algorithm is used for track control. In addition to the yaw moment layer, the PID algorithm and SMC algorithm are used to realize the speed tracking and yaw angle speed tracking control. In the driving moment distribution layer, the direct wheel slip rate control and the optimal driving moment distribution are realized using the optimal distribution algorithm and PID control algorithm. By integrating these layers, our approach improves the precision of trajectory-following while ensuring the vehicle's yaw stability.
- (2) This paper focuses on the influence of direct slip rate control on vehicle trajectory tracking and yaw stability. One method of setting the optimal slip rate threshold control was proposed. The driving torque of the target was transformed into the ideal slip rate using the inverse tire model. The actual slip rate tracked the ideal slip rate using the PID control method, which finally improved the vehicle trajectory tracking and stability control.
- (3) Building upon existing research, this paper proposes the incorporation of vehicle speed control and tire direct slip rate control, followed by a comparative analysis with previous findings. The discoveries from this study have significant implications for the enhancement of vehicle control systems and ensure an enhanced driving experience for motorists.

The proposed paper is structured as follows: Section 2 introduces the modeling of vehicle dynamics, while Section 3 presents a comprehensive control method for trajectory tracking, yaw stability, and tire longitudinal force (sliding rate). Section 4 presents the simulation results and a comparative analysis, and, finally, the conclusion is drawn.

Note: In Section 4, the simulation results of the proposed control strategy and algorithm are labeled as integrated control. The simulation results of similar studies have been labeled as general control.

## 2. Vehicle Dynamics Modeling

This study is centered on the investigation of a front-wheel-steering four-wheel hub electric vehicle with a distributed architecture. A distinctive characteristic of this vehicle type is the absence of conventional mechanical power transmission gadgets, and, instead, the use of four hub motors to drive each wheel independently, resulting in enhanced flexibility and control. Figure 1 illustrates the system structure diagram of the electric vehicle with distributed four-wheel hub motors.

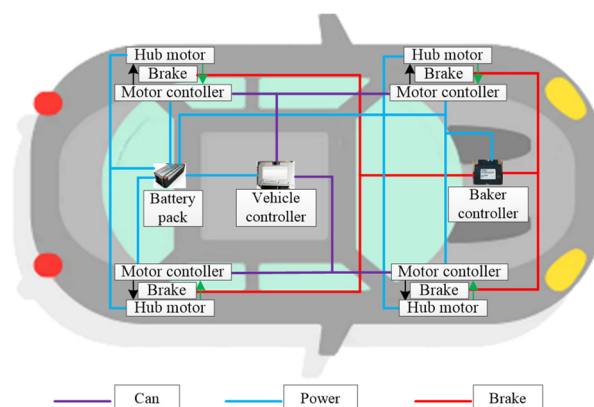


**Figure 1.** Distributed four-wheel hub electric vehicle system structure.

To assess the dynamic features of the automobile when it follows a given path, an all-inclusive vehicle dynamics model was formulated, taking into account the vehicle's lateral, longitudinal, and yaw directions, as depicted in Figure 2.

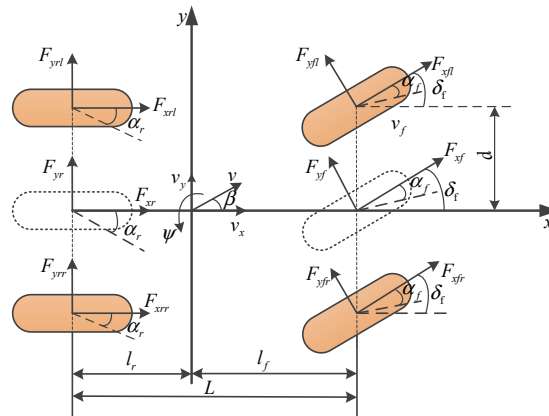


Figure 2. Vehicle dynamics model considering path tracking.

With the intention of accurately capture the vehicle’s dynamic behavior during path monitoring, a comprehensive vehicle dynamic model was developed, which considers the lateral, longitudinal, and yaw dynamics of a vehicle, as depicted in Figure 2. However, to ensure that the modeling results are accurate, certain assumptions were made. These assumptions include neglecting the impact of air resistance, treating the vehicle as a rigid body and ignoring its vertical, pitch, and roll motions, and assuming that the front wheel angle remains constant without considering the influence of the steering system. Since this paper focuses on the dynamic characteristics of a distributed four-wheel hub EV with front-wheel steering, only the front-wheel steering  $\delta_f$  is considered in the analysis.

Based on Figure 2 and the aforementioned assumptions, the vehicle dynamic balance equation is established as follows:

$$\begin{cases} m(\ddot{x} - \dot{y}\dot{\psi}) = (F_{xfl} + F_{xfr}) \cos \delta_f - (F_{yfl} + F_{yfr}) \sin \delta_f + (F_{xxl} + F_{xrr}) \\ m(\ddot{y} + \dot{x}\dot{\psi}) = (F_{xfl} + F_{xfr}) \sin \delta_f + (F_{yfl} + F_{yfr}) \cos \delta_f + (F_{yrl} + F_{yrr}) \\ I_z \ddot{\psi} = l_f((F_{xfl} + F_{xfr}) \sin \delta_f + (F_{yfl} + F_{yfr}) \cos \delta_f) - l_r(F_{yrl} + F_{yrr}) \end{cases} \quad (1)$$

where  $m$  represents the vehicle mass;  $x, y$  represent the vehicle’s longitudinal and lateral displacements;  $\psi$  is the vehicle yaw angle;  $\delta_f$  is the steering angle of the front wheels;  $I_z$  is the vehicle’s z-axis moment of inertia;  $l_f, l_r$  are, respectively, the longitudinal distance between the center of mass and the front and rear axles;  $F_{xfl}, F_{xfr}, F_{xrl}$  and  $F_{xrr}$  represent the longitudinal forces on the four wheels;  $F_{yfl}, F_{yfr}, F_{yrl}$  and  $F_{yrr}$  represent the lateral forces acting on all four tires;  $M_x$  is the additional yaw moment.

The magic formula model has gained popularity due to its unified structure and high precision in calculating the longitudinal and lateral forces of tires during vehicle operation [31]. This makes it an ideal tool for analyzing the dynamic behavior of vehicles. Specifically, the magic tire model is used to calculate the longitudinal force of a tire during pure longitudinal slip, which is essential for accurately modeling the vehicle’s behavior during trajectory tracking.

$$\begin{cases} F_{xi} = D_x \sin\{C_x \arctan[B_x S_i - E_x(B_x S_i - \arctan(B_x S_i))]\} \\ C_x = a_0 \\ D_x = a_1 F_{zi}^2 + a_2 F_{zi} \\ B_x = (a_3 F_{zi}^2 + a_4 F_{zi}) \exp(-a_5 F_{zi}) / (C_x D_x) \\ E_x = a_6 F_{zi}^2 + a_7 F_{zi} + a_8 \end{cases} \quad (2)$$

where  $i = fl, fr, rl, rr$  indicates the front-left, front-right, rear-left, and rear-right wheels;  $F_{zi}$  refers to the weight supported by each of the four tire wheels in a vertical direction;  $S_i$  is the tire sliding rate.

Tire lateral force under pure deflection condition is

$$\begin{cases} F_{yi} = D_y \sin\{C_y \arctan[B_y \alpha_i - E_y (B_y \alpha_i - \arctan(B_y \alpha_i))]\} \\ C_y = b_0 \\ D_y = b_1 F_{zi}^2 + b_2 F_{zi} \\ B_y = b_3 \sin(b_4 \arctan(b_5 F_{zi})) / (C_y D_y) \\ E_y = b_6 F_{zi}^2 + b_7 F_{zi} + b_8 \end{cases} \quad (3)$$

where  $\alpha_i$  is the angle of sideways bending of the tire.

In situations where the tire is experiencing both sliding and sideslip, the tire is considered to be in a combined working condition. In such cases, the tire force can be determined using the following formula [32]:

$$\begin{cases} F_{xi} = \frac{-S_i}{\sqrt{S_i^2 + (\tan \alpha_i)^2}} D_x^* \sin\{C_x^* \arctan[B_x^* S_i - E_x (B_x^* S_i - \arctan(B_x^* S_i))]\} \\ F_{yi} = \frac{-\tan \alpha_i}{\sqrt{S_i^2 + (\tan \alpha_i)^2}} D_y^* \sin\{C_y^* \arctan[B_y^* \alpha_i - E_y (B_y^* \alpha_i - \arctan(B_y^* \alpha_i))]\} \end{cases} \quad (4)$$

where  $\begin{cases} D_x^* = \mu D_x \\ C_x^* = (\frac{5}{4} - \frac{\mu}{4}) C_x \\ B_x^* = (2 - \mu) B_x \end{cases}, \begin{cases} D_y^* = \mu D_y \\ C_y^* = (\frac{5}{4} - \frac{\mu}{4}) C_y \\ B_y^* = (2 - \mu) B_y \end{cases}$ ,  $\mu$  is the road adhesion coefficient.

The actual longitudinal sliding rate of the vehicle in the running state is:

$$S_i = \begin{cases} (1 - \frac{v_i}{\omega_i r}) \times 100\% > 0 & \omega_i r \geq v_i \\ (\frac{\omega_i r}{v_i} - 1) \times 100\% < 0 & \omega_i r < v_i \end{cases} \quad (5)$$

where  $v_i$  is the velocity of the center of each wheel;  $\omega_i$  is the rotational speed of each wheel.

The angular velocity of each wheel can be represented as:

$$\begin{cases} v_{fl} = (v_x - \frac{1}{2} d_f \cdot \dot{\psi}) \cdot \cos \delta_f + (v_y + l_f \cdot \dot{\psi}) \cdot \sin \delta_f \\ v_{fr} = (v_x + \frac{1}{2} d_f \cdot \dot{\psi}) \cdot \cos \delta_f + (v_y + l_f \cdot \dot{\psi}) \cdot \sin \delta_f \\ v_{rl} = v_x - \frac{1}{2} d_r \cdot \dot{\psi} \\ v_{rr} = v_x + \frac{1}{2} d_r \cdot \dot{\psi} \end{cases} \quad (6)$$

where  $v_x$  is the forward velocity;  $v_y$  is centroid lateral velocity;  $\dot{\psi}$  is the yaw angular velocity;  $d_f$  is front wheel pitch;  $d_r$  is the rear wheel pitch.

The lateral inclination angle of every tyre is:

$$\begin{cases} \alpha_{fl} = \delta_f - \arctan\left(\frac{v_y + l_f \cdot \dot{\psi}}{v_x - \frac{1}{2} d_f \cdot \dot{\psi}}\right) \\ \alpha_{fr} = \delta_f - \arctan\left(\frac{v_y + l_f \cdot \dot{\psi}}{v_x + \frac{1}{2} d_f \cdot \dot{\psi}}\right) \\ \alpha_{rl} = \arctan\left(\frac{l_f \cdot \dot{\psi} - v_y}{v_x - \frac{1}{2} d_r \cdot \dot{\psi}}\right) \\ \alpha_{rr} = \arctan\left(\frac{l_f \cdot \dot{\psi} - v_y}{v_x + \frac{1}{2} d_r \cdot \dot{\psi}}\right) \end{cases} \quad (7)$$

During the actual operation of a vehicle, changes in longitudinal and lateral acceleration can cause variations in the vehicle's vertical load, which can be expressed as [33]:

$$\begin{cases} F_{zfr} = \frac{m}{2L} \left( gl_r - a_x h - \frac{a_y h l_r}{d_f} \right) \\ F_{zfl} = \frac{m}{2L} \left( gl_r - a_x h + \frac{a_y h l_r}{d_f} \right) \\ F_{zrl} = \frac{m}{2L} \left( gl_f + a_x h - \frac{a_y h l_f}{d_r} \right) \\ F_{zrr} = \frac{m}{2L} \left( gl_f + a_x h + \frac{a_y h l_f}{d_r} \right) \end{cases} \quad (8)$$

where  $F_{zfl}$ ,  $F_{zfr}$ ,  $F_{zrl}$  and  $F_{zrr}$  indicate the vertical force applied on the left-front, right-front, left-rear, and right-rear wheels, respectively;  $l_r$  refers to the distance from the vehicle's center of mass to the center of the rear wheels;  $l_f$  refers to the distance from the vehicle's center of mass to the center of the front wheels;  $d_f$  is half the distance between the front wheels;  $d_r$  is half the distance between the rear wheels;  $a_x$ ,  $a_y$  are, respectively, the wheel's acceleration in the longitudinal and lateral directions;  $h$  is referred to as the center of mass height.

By analyzing the transformation relationship between the car's reference frame and the Earth's reference frame, we can derive the following result:

$$\begin{cases} \dot{Y} = \dot{x} \sin \varphi + \dot{y} \cos \varphi \\ \dot{X} = \dot{x} \cos \varphi - \dot{y} \sin \varphi \end{cases} \quad (9)$$

where  $X$  and  $Y$ , respectively, are the longitudinal displacement and lateral displacement of the vehicle in the geodetic coordinate system.

Given the 3-DOF four-wheel model of the vehicle represented in Figure 2 and the theoretical analysis presented above, the vehicle dynamics model can be established assuming small angles in the front wheels.

$$\begin{cases} \ddot{x} = \dot{y} \dot{\varphi} + \frac{1}{m} \left[ F_{xfl} + F_{xfr} - (F_{yfl} + F_{yfr}) \delta_f + F_{xrl} + F_{xrr} \right] \\ \ddot{y} = -\dot{x} \dot{\varphi} + \frac{1}{m} \left[ (F_{xfl} + F_{xfr}) \delta_f + F_{yfl} + F_{yfr} + F_{yrl} + F_{yrr} \right] \\ \ddot{\varphi} = \frac{1}{I_z} \left[ l_f \left( (F_{xfl} + F_{xfr}) \delta_f + F_{yfl} + F_{yfr} \right) - l_r \left( F_{yrl} + F_{yrr} \right) \right] \\ \dot{\varphi} = \dot{\varphi} \\ \dot{Y} = \dot{x} \sin \varphi + \dot{y} \cos \varphi \\ \dot{X} = \dot{x} \cos \varphi - \dot{y} \sin \varphi \end{cases} \quad (10)$$

where  $\ddot{x}$  represents the longitudinal acceleration of the vehicle;  $\ddot{y}$  represents the lateral acceleration of the vehicle.

To streamline the vehicle path following and yaw control, the three-dimensional model of the four-wheeled vehicle was simplified to a two-dimensional model of a single wheel. To effectively enhance the vehicle's driving performance on low-adhesion road surfaces, this study incorporates the vehicle slip rate  $S$  into the nonlinear model as a control variable to regulate the wheel slip rate.

Assuming that the sideslip angle and sliding rate are at their minimum, the tire force can be approximated by a linear function. In addition, when the front-wheel steering angle is small and the tire is in a linear region, the tire's longitudinal and lateral forces can be represented as [34]:

$$\begin{cases} F_{xf} = 2C_f S_f \\ F_{xr} = 2C_r S_r \\ F_{yf} = 2k_f \alpha_f \\ F_{yr} = 2k_r \alpha_r \end{cases} \quad (11)$$

$$\begin{cases} S_f = \max\{|S_{fl}|, |S_{fr}|\} \\ S_r = \max\{|S_{rl}|, |S_{rr}|\} \end{cases} \tag{12}$$

$$\begin{cases} \alpha_f = \frac{\dot{y} + l_f \dot{\varphi}}{\dot{x}} - \delta_f \\ \alpha_r = \frac{\dot{y} - l_r \dot{\varphi}}{\dot{x}} \end{cases} \tag{13}$$

where  $C_f$  and  $C_r$  are the longitudinal stiffness of front and rear tires;  $k_f$  and  $k_r$  are the lateral stiffness of front and rear tires;  $S_f$  and  $S_r$  are the longitudinal sliding rate of front and rear tires;  $\alpha_f$  and  $\alpha_r$  are front and rear tire side angle, respectively.

The vehicle's vehicle dynamics equation is simplified into a monorail model, which allows for a more streamlined approach to analyzing the vehicle's behavior. Additionally, the vehicle body coordinate system is converted to a Cartesian coordinate system, further simplifying the model. By incorporating these changes, a comprehensive, nonlinear model of the vehicle's dynamics can be developed. This model takes into account a range of factors, including vehicle weight, tire friction, and road conditions, enabling more accurate predictions of the vehicle's behavior and movement.

$$\begin{cases} \ddot{y} = -\dot{x}\dot{\varphi} + \frac{2}{m} \left[ C_f S_f \delta_f + k_f \left( \delta_f - \frac{\dot{y} + l_f \dot{\varphi}}{\dot{x}} \right) + k_r \frac{l_r \dot{\varphi} - \dot{y}}{\dot{x}} \right] \\ \ddot{x} = \dot{y}\dot{\varphi} + \frac{2}{m} \left[ C_f S_f - k_f \delta_f \left( \delta_f - \frac{\dot{y} + l_f \dot{\varphi}}{\dot{x}} \right) + C_r S_r \right] \\ \dot{\varphi} = \gamma \\ \ddot{\varphi} = \frac{2}{I_z} \left[ l_f \left( C_f S_f \delta_f + k_f \left( \delta_f - \frac{\dot{y} + l_f \dot{\varphi}}{\dot{x}} \right) \right) - l_r k_r \frac{l_r \dot{\varphi} - \dot{y}}{\dot{x}} \right] \\ \dot{Y} = \dot{x} \sin \varphi + \dot{y} \cos \varphi \\ \dot{X} = \dot{x} \cos \varphi - \dot{y} \sin \varphi \end{cases} \tag{14}$$

### 3. Controller Design

Figure 3 illustrates the control framework designed for tracking the trajectory of an electric vehicle (EV) equipped with distributed four-wheel hubs. The control structure comprises three levels: upper MPC trajectory tracking control, middle sliding mode yaw moment control, and lower driving moment optimal distribution. These levels work together in a multi-closed-loop system to achieve an accurate trajectory tracking and ensure the yaw stability of the vehicle. The integration of these control strategies ensures that the estimation of vehicle tracking is both precise and stable. The proposed architecture enhances the overall performance and safety of the EV.

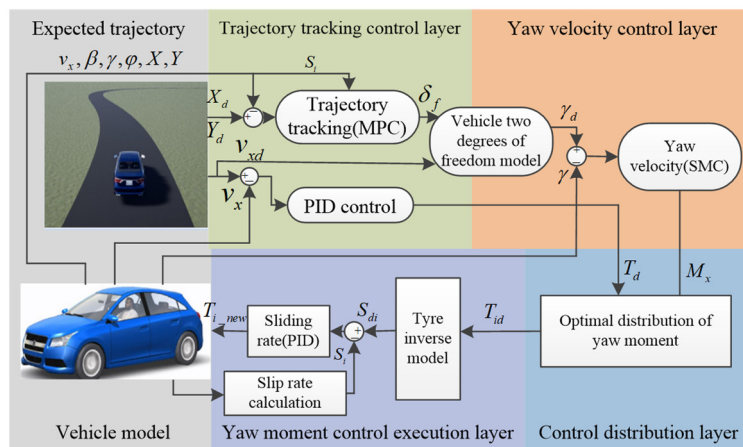


Figure 3. Integrated control strategy of trajectory tracking and control stability based on MPC.

In the upper layer, the MPC controller outputs the expected front wheel angle  $\delta_f$  based on the desired path information, the vehicle's own posture, and the vehicle dynamics model. If the actual speed  $v_x$  and expected speed  $v_{xd}$  of the vehicle deviate, the PID speed controller intervenes to ensure actual speed  $v_x$  control, achieve the desired speed  $v_{xd}$  tracking, and produce the overall the vehicle's driving force  $T_d$ . In the intermediate-level yaw torque regulation, the upper control's determination of the front wheel angle  $\delta_f$  and velocity  $v_{xd}$ , in conjunction with the desired yaw rate  $\gamma_d$  generated by the two-degree-of-freedom model of the vehicle, are utilized. If the desired yaw velocity  $\gamma_d$  differs greatly from the actual yaw velocity  $\gamma$  of the vehicle, the yaw stability controller based on the sliding mode control algorithm intervenes and outputs additional yaw torque  $M_x$ . The lower level employs a torque optimization algorithm to distribute the desired longitudinal force  $F_x$  among the four wheels, thereby achieving the calculated longitudinal driving torque  $T_d$  and extra yaw torque  $M_x$ . It converts the target longitudinal torque  $F_x$  into the target longitudinal sliding rate  $S_{di}$  by utilizing the inverse tire model and employing the sliding rate calculation module; then, the current sliding rate  $S_i$  of the vehicle is accurately determined. It then compares the target longitudinal sliding rate  $S_{di}$  to realize the wheel sliding rate control and finally achieves the longitudinal force control of the vehicle tire.

### 3.1. Trajectory Tracking Control

The core idea behind model predictive control (MPC) is to use the current system state, available model, and future control inputs to anticipate the future output. By utilizing rolling optimization, MPC can solve the constrained optimization problem, incorporating the characteristics of model prediction, rolling optimization, and feedback correction. To establish a prediction model for the MPC controller, the three-degrees-of-freedom nonlinear dynamics model system's state space equation is simplified to create a reliable forecasting model for the vehicle. It is crucial to consider the nonlinear dynamics of the actual system and incorporate appropriate control design strategies to achieve the desired performance.

$$\begin{cases} \dot{\zeta} = f(\zeta(t), u(t)) \\ y = C\zeta(t) \end{cases} \quad (15)$$

where the state variable is chosen as  $\zeta = [\dot{y} \quad \dot{x} \quad \varphi \quad \gamma \quad Y \quad X]$ . The control quantity is selected as  $u = \delta_f$ . The output is selected as  $y = [\varphi \quad Y]$ . In the actual control process, the coefficient of friction  $\mu$  between the road surface and the vehicle is regarded as the known quantity according to the road condition, and the sliding rate  $S$  is regarded as the control quantity.

For the nonlinear vehicle dynamics model, the forward Euler method is adopted for discretization at time  $k$ :

$$\frac{\zeta(k+1) - \zeta(k)}{T} = f(\zeta(k), u(k)) \quad (16)$$

where  $T$  is the model's predicted sampling time for the controller;  $k$  is the predicted sampling time for walking a long distance.

Taylor formula is used to linearize and simplify the discrete nonlinear model, and is written in incremental form as:

$$\begin{aligned} \zeta(k+1) &= A_{k,t}\zeta(k) + B_{k,t}u(k) + d_{k,t} \\ d_{k,t} &= \hat{\zeta}_t(k+1) - A_{k,t}\hat{\zeta}_t(k) - B_{k,t}u_t(k) \end{aligned} \quad (17)$$

This can be further rewritten into:

$$\begin{aligned} \zeta_{new}(k+1|t) &= A\zeta_{new}(k|t) + B\Delta u(k|t) + d_k \\ y_{new}(k|t) &= c_{new}\zeta_{new}(k|t) \end{aligned} \quad (18)$$

where  $A = \begin{bmatrix} A_{k,t} & B_{k,t} \\ 0 & 1 \end{bmatrix}$ ,  $B = \begin{bmatrix} B_{k,t} \\ 1 \end{bmatrix}$ ,  $d_k = \begin{bmatrix} d_{k,t} \\ 0 \end{bmatrix}$ ;  $C$  is the output matrix.

To establish the prediction model for the MPC controller, some assumptions are made to simplify the calculation. It is assumed that the prediction time horizon for the MPC controller is  $N_p$ , and the control time horizon is  $N_c$ , where  $N_c$  is less than or equal to  $N_p$ . It is possible to infer the state of the vehicle system within the prediction time window based on its current state and output.

$$\begin{aligned} A_{k,t} &= A_{t,t}, k = 1, 2, \dots, t + N - 1 \\ B_{k,t} &= B_{t,t}, k = 1, 2, \dots, t + N - 1 \\ d_{k,t} &= d_{t,t}, k = 1, 2, \dots, t + N - 1 \end{aligned} \tag{19}$$

From the present state and output, we can infer the state of the vehicle system in the prediction time interval:

$$\begin{cases} \zeta_{new}(t + 1|t) = A\zeta_{new}(t|t) + B\Delta u(t|t) + d_t \\ \zeta_{new}(t + 2|t) = A^2\zeta_{new}(t|t) + AB\Delta u(t|t) + B\Delta u(t + 1|t) + Ad_t + d_{t+1} \\ \zeta_{new}(t + 3|t) = A^3\zeta_{new}(t|t) + A^2B\Delta u(t|t) + AB\Delta u(t + 1|t) + B\Delta u(t + 2|t) + A^2d_t + Ad_{t+1} + d_{t+2} \\ \dots \\ \zeta_{new}(t + N_p|t) = A^{N_p}\zeta_{new}(t|t) + A^{N_p-1}B\Delta u(t|t) + \dots + B\Delta u(t + N_c - 1|t) + A^{N_p-1}d_t + A^{N_p-2}d_{t+1} + \dots + d_{t+N_p-1} \end{cases} \tag{20}$$

The future output can be predicted by analyzing the current state and output:

$$Y(t) = \begin{bmatrix} y_{new}(t + 1|t) \\ y_{new}(t + 2|t) \\ y_{new}(t + 3|t) \\ \dots \\ y_{new}(t + N_p|t) \end{bmatrix} = C_{new} \begin{bmatrix} \zeta_{new}(t + 1|t) \\ \zeta_{new}(t + 2|t) \\ \zeta_{new}(t + 3|t) \\ \dots \\ \zeta_{new}(t + N_p|t) \end{bmatrix} \tag{21}$$

Write this as a matrix:

$$Y(t) = \psi_t \zeta_{new}(t) + \theta_t \Delta U(t) + \Gamma_t \phi(t) \tag{22}$$

where  $\psi_t = [C_{new}A \ C_{new}A^2 \ \dots \ C_{new}A^{N_p}]^T$ ,  $\Delta U(t) = [\Delta u(t|t) \ \Delta u(t + 1|t) \ \dots \ \Delta u(t +$

$$N_c - 1|t)]^T$$
,  $\phi(t) = [d_t \ d_{t+1} \ \dots \ d_{t+N_p-1}]^T$ ,  $\Gamma_t = \begin{bmatrix} C_{new} & 0 & 0 & 0 \\ C_{new}A & C_{new} & 0 & 0 \\ C_{new}A^2 & C_{new}A & C_{new} & 0 \\ \dots & \dots & \dots & \dots \\ C_{new}A^{N_p-1} & C_{new}A^{N_p-2} & \dots & C_{new} \end{bmatrix}$ ,

$$\theta_t = \begin{bmatrix} C_{new}B & 0 & 0 & 0 \\ C_{new}AB & C_{new}B & 0 & 0 \\ C_{new}A^2B & C_{new}AB & C_{new}B & 0 \\ \dots & \dots & \dots & \dots \\ C_{new}A^{N_p-1}B & C_{new}A^{N_p-2}B & \dots & C_{new}A^{N_p-N_c}B \end{bmatrix}$$

The objective function of the predictive model controller can be formulated as follows:

$$J = \sum_{i=1}^{N_p} \left\| y(t + i|t) - y_{ref}(t + i|t) \right\|_Q^2 + \sum_{i=0}^{N_c-1} \left\| \Delta u(t + i|t) \right\|_R^2 + \rho \varepsilon^2 \tag{23}$$

where  $y(t + i|t) - y_{ref}(t + i|t)$  represents the discrepancy between the current output state and the reference state of the system;  $Q$  is the matrix that represents the weightage given to the tracking precision;  $\Delta u(t + i|t)$  denotes the control increment;  $R$  is the matrix representing the weight assigned to the control variation;  $\varepsilon$  represents the relaxation factor; and  $\rho$  is the weight coefficient of the relaxation factor.

To convert the objective function into a quadratic term, we need to express the tracking error and control increment in terms of the state variables. This can be achieved using the system dynamics equations and the control law. Once we have expressions for the tracking

error and control increment in terms of the state variables, we can substitute them into the objective function and expand this to obtain a quadratic term. The resulting quadratic form can then be minimized using standard optimization techniques.

$$J = [Y(t) - Y_{ref}(t)]^T \bar{Q} [Y(t) - Y_{ref}(t)] + \Delta U(t)^T \bar{R} \Delta U(t) + \varepsilon^T \rho \varepsilon \quad (24)$$

where  $Y_{ref}(t) = [y_{ref}(t+1|t) \ y_{ref}(t+2|t) \ \dots \ y_{ref}(t+N_p|t)]^T$ ,  $y_{ref} = [\varphi \ Y]^T$  denotes the anticipated control input in the predicted time horizon.

The objective function is composed of three terms. The first term guarantees the accuracy of the desired path tracking by regulating the vehicle's lateral and course deviation. The second term reduces the control increment, i.e., the change in the angle of the front wheels and the additional yaw torque, in order to preserve the intelligent vehicle's stable steering performance. The third component represents the relaxation factor, which is managed by the relaxation factor and weight coefficient to strike a balance between the tracking accuracy and control effort.

Convert the objective function into a quadratic term in the following form:

$$J = \frac{1}{2} \begin{bmatrix} \Delta U(t) \\ \varepsilon \end{bmatrix}^T H \begin{bmatrix} \Delta U(t) \\ \varepsilon \end{bmatrix} + f^T \begin{bmatrix} \Delta U(t) \\ \varepsilon \end{bmatrix} \quad (25)$$

where  $H = \begin{bmatrix} 2(\theta_t^T \bar{Q} \theta_t + \bar{R}) & 0 \\ 0 & 2\rho \end{bmatrix}$ ,  $f^T = [-2E(t)^T \bar{Q} \theta_t \ 0]$ .

To account for the limitations of the mechanical actuator and vehicle's dynamic behavior, it is crucial to establish constraints on control quantity, control increment, and system output. Such constraints may include:

$$\begin{cases} U_{\min} \leq U_t + A_I \Delta U_t \leq U_{\max} \\ \Delta U_{\min} \leq \Delta U_t \leq \Delta U_{\max} \\ Y_{\min} \leq Y \leq Y_{\max} \end{cases} \quad (26)$$

This can be achieved by using quadratic programming (QP), which facilitates the identification of an optimal control increment sequence within the control time domain while accounting for the vehicle's mechanical actuator and dynamic performance limitations.

$$\Delta U(t) = [\Delta u(t), \Delta u(t+1), \dots, \Delta u(t+N_c-1)]^T \quad (27)$$

In each control cycle, the initial element of the optimal control sequence is implemented as the actual control input increment to the system:

$$u(t) = u(t-1) + \Delta u(t) \quad (28)$$

The front wheel angle  $\delta_f$  obtained from the optimization solution is directly fed into the lower torque optimization distribution layer as the expected front wheel angle, taking into account the limitations of the vehicle's mechanical actuator and dynamic performance.

### 3.2. Longitudinal Velocity PID Control

To ensure that the actual longitudinal vehicle speed  $v_x$  follows the reference longitudinal vehicle speed  $v_{xd}$ , a PID control method is employed due to its simplicity in control system design and high computational efficiency. This method is widely used in industrial control. Therefore, in order to reduce calculation costs, PID control is chosen as a speed tracking control.

$$u(t) = K_p e(t) + K_i \int_0^t e(t) dt + K_D \frac{de(t)}{dt} \quad (29)$$

where  $e(t) = v_{xd} - v_x$  refers to the difference between the desired velocity and the current velocity of the vehicle;  $u(t) = T_d$  is the ideal total driving moment.

### 3.3. Yaw Stability Control

In order to achieve effective trajectory tracking control, it is crucial to design a suitable yaw stability controller that takes the vehicle’s stability into consideration. In this study, a sliding mode control algorithm was employed to design the yaw stability controller, which is responsible for calculating the additional yaw moment required to maintain the vehicle’s stability. The ideal yaw velocity was obtained from a two-degrees-of-freedom vehicle model [35].

$$\gamma_0 = \frac{v_x}{L(1 + kv_x^2)} \delta_f \tag{30}$$

where the stability factor is as follows:  $k = \frac{m}{L^2} (\frac{l_f}{k_r} - \frac{l_r}{k_f})$ .

Considering the limited traction provided by the ground, the maximum limit of yaw velocity has been restricted to [34]:

$$|\gamma_{\max}| = 0.85 \frac{\mu g}{v_x} \tag{31}$$

The expected value of the resulting yaw velocity is as follows:

$$\gamma_d = \min\{|\gamma_0|, |\gamma_{\max}|\} \text{sgn}(\gamma_0) \tag{32}$$

To achieve the desired yaw speed tracking control without taking into account external disturbances, a sliding mode control algorithm was developed to calculate the required additional yaw moment of the vehicle. According to the actual yaw velocity value of the vehicle  $\gamma$ , make  $s = \gamma - \gamma_d$ , take  $\dot{s} = 0$ , and obtain:  $\dot{s} = \dot{\gamma} - \dot{\gamma}_d = 0$ .

where  $\dot{\gamma} = \frac{1}{I_z} \{l_f(F_{yfl} + F_{yfr}) \cos \delta_f - l_r(F_{yrl} + F_{yrr}) + d_f(F_{yfl} - F_{yfr}) \sin \delta_f + M_x\}$ .

The equivalent control item is designed as follows:

$$M_{xeq} = I_z \dot{\gamma} - \{l_f(F_{yfl} + F_{yfr}) \cos \delta_f - l_r(F_{yrl} + F_{yrr}) + d_f(F_{yfl} - F_{yfr}) \sin \delta_f\} \tag{33}$$

In order to achieve this,  $s\dot{s} < 0$  is established. The switch robust control is designed as:

$$M_{xsw} = I_z K \text{sgn}(s) \tag{34}$$

where  $K$  is sliding mode switching gain,  $K = D + \eta$ .

Equivalent synovial control law is as follows:

$$M_x = I_z \dot{\gamma} - \{l_f(F_{yfl} + F_{yfr}) \cos \delta_f - l_r(F_{yrl} + F_{yrr}) + d_f(F_{yfl} - F_{yfr}) \sin \delta_f\} + I_z K \text{sgn}(s) \tag{35}$$

In order to eliminate chattering, a quasi-sliding mode control is adopted, and the saturation function  $\text{sat}(s)$  is used instead of the sign function [36]:

$$\text{sat}(s) = \begin{cases} 1, & s > \phi \\ \frac{s}{\phi}, & |s| \leq \phi \\ -1, & s < -\phi \end{cases} \tag{36}$$

where  $\phi$  is the boundary layer, and is a constant greater than zero.

### 3.4. Optimal Torque Distribution

The first step in optimizing torque allocation is to select an objective function for optimization. The focus is on maximizing the tire’s adhesion ability and utilization. To ensure stability in vehicle handling, the “attachment ellipse” theory is employed to keep the range of lateral and longitudinal forces of the tire within the boundary of the attachment

ellipse. Although the lateral force of the tire cannot be directly controlled, the longitudinal force can be controlled. Therefore, the primary optimization objective is to minimize the comprehensive adhesion utilization of all four wheels. This paper simplifies the objective function to minimize the sum of squares of the longitudinal attachment utilization of the four wheels, disregarding the lateral force based on the “attachment ellipse” theory.

$$\min J_1 = \sum_{i=fl,fr,rl,rr} \frac{T_{id}^2}{(r\mu F_{zi})^2} \tag{37}$$

where  $T_{id}$  represents the target driving torque generated by the four hub motors of the vehicle;  $\mu$  is the adhesion coefficient of four wheels touching the ground.

To maintain the stability of the vehicle, it is necessary to adjust the longitudinal force of the four wheels through weight allocation, indirectly controlling the sideways force. This is achieved by minimizing the comprehensive adhesion utilization of all four wheels, with the objective of keeping the range of lateral and longitudinal forces within the boundary of the attachment ellipse. The weight distribution plan employed in this paper is founded based on the vehicle’s running and stress characteristics, with a small weight for the front wheel and a large weight for the rear wheel. The front wheel weight is fixed at 1, while the upper limit value of the rear wheel weight is set at 2. The size is adjusted based on the deviation of the yaw velocity, and the weight of the front and rear wheels is determined accordingly [37].

$$\begin{cases} c_{fl} = c_{fr} = 1 \\ c_{rl} = c_{rr} = 1 & \Delta\gamma \leq 0 \\ c_{rl} = c_{rr} = 1 + 1.25\Delta\gamma & 0 \leq \Delta\gamma \leq 0.08 \\ c_{rl} = c_{rr} = 2 & \Delta\gamma \geq 0.08 \end{cases} \tag{38}$$

Therefore, the optimization expression of longitudinal attachment utilization under dynamic weight allocation is as follows:

$$\min J_1 = \sum_{i=fl,fr,rl,rr} c_i \frac{T_{id}^2}{(r\mu F_{zi})^2} = u^T Q u \tag{39}$$

where  $u = [T_{fld} \ T_{frd} \ T_{rld} \ T_{rrd}]^T$ ,  $Q = \text{diag}\left(\frac{c_{fl}}{(r\mu F_{zfl})^2} \ \frac{c_{fr}}{(r\mu F_{zfr})^2} \ \frac{c_{rl}}{(r\mu F_{zrl})^2} \ \frac{c_{rr}}{(r\mu F_{zrr})^2}\right)$ ,  $c_{fl}$ ,  $c_{fr}$ ,  $c_{rl}$ ,  $c_{rr}$  is the weight distribution coefficient of the driving torque for the four-wheel hub motor;  $r$  is the radius of the wheel.

In order to reduce the longitudinal force distribution error, the tracking of the total driving moment  $T_d$  and additional yaw moment  $M_x$  of the upper layer motion control is added to the objective optimization function, so that the actual execution signal of the wheel hub motor is as consistent as possible with the expected control signal output of the upper layer controller.

$$\min J_2 = \lambda_1 \left(C^T u - \frac{T_d}{r}\right)^T \left(C^T u - \frac{T_d}{r}\right) + \lambda_2 (G^T u - M_x)^T (G^T u - M_x) \tag{40}$$

where  $C^T = \begin{bmatrix} \frac{\cos \delta_f}{r} & \frac{\cos \delta_f}{r} & \frac{1}{r} & \frac{1}{r} \end{bmatrix}$ ,  $G = \begin{bmatrix} \frac{-d \cos \delta_f + l_f \sin \delta_f}{r} \\ \frac{d \cos \delta_f + l_f \sin \delta_f}{r} \\ \frac{d_f}{r} \\ \frac{d_r}{r} \end{bmatrix}$ ,  $T_d$  is the total expected longitudinal moment output by the driver’s speed controller, and  $M_x$  is the expected yaw moment output by the yaw stability controller.  $\lambda_1$  and  $\lambda_2$  are the weight coefficients. The priority of the target control torque can be determined by adjusting the weight coefficients  $\lambda_1$  and  $\lambda_2$ .

The objective optimization function of optimal torque distribution is designed as follows:

$$\min J = J_1 + J_2 = u^T Q u + \lambda_1 \left( C^T u - \frac{T_d}{r} \right)^T \left( C^T u - \frac{T_d}{r} \right) + \lambda_2 \left( G^T u - M_x \right)^T \left( G^T u - M_x \right) \quad (41)$$

Convert the objective optimization function into quadratic form as follows:

$$\min J = \frac{1}{2} u^T \left( 2Q + 2\lambda_1 C C^T + 2\lambda_2 G G^T \right) u + \left( -2\lambda_1 C^T \frac{T_d}{r} - 2\lambda_2 G^T M_x \right) u + k_1 \left( \frac{T_d}{r} \right)^2 + k_2 M_x^2 \quad (42)$$

As the term  $\lambda_1 \left( \frac{T_d}{r} \right)^2 + \lambda_2 M_x^2$  independent of the final result, the objective optimization function is reduced to the following form:

$$\min J = \frac{1}{2} u^T \left( 2Q + 2\lambda_1 C C^T + 2\lambda_2 G G^T \right) u + \left( -2\lambda_1 C^T \frac{T_d}{r} - 2\lambda_2 G^T M_x \right) u \quad (43)$$

The expected longitudinal torque of the wheel should meet the road adhesion conditions, and the longitudinal torque should be within the maximum driving range of the hub motor. Therefore, the constraint expression is:

$$s.t. \begin{cases} -r\mu F_{zi} \leq T_{id} \leq \min(r\mu F_{zi}, T_{id,max}) \\ T_d = T_{fld} + T_{rld} + T_{frd} + T_{rrd} \end{cases} \quad (44)$$

where  $T_i$  is the torque generated by an individual hub motor;  $T_{i,max}$  is the maximum torque that can be provided by the hub motor at the current speed.

The target longitudinal tire torque distribution problem based on objective optimization can be expressed as:

$$\begin{cases} \min J = u^T \left( 2Q + 2\lambda_1 C C^T + 2\lambda_2 G G^T \right) u + \left( -2\lambda_1 C^T \frac{T_d}{r} - 2\lambda_2 G^T M_x \right) u \\ s.t. \quad -r\mu F_{zi} \leq T_{id} \leq \min(r\mu F_{zi}, T_{id,max}) \\ T_d = T_{fld} + T_{rld} + T_{frd} + T_{rrd} \end{cases} \quad (45)$$

To solve the problem and achieve the optimal distribution of longitudinal torque, the quadratic programming method is utilized based on the aforementioned objective and constraint conditions. This method provides the ideal longitudinal torque for each wheel to ensure the maximum comprehensive adhesion utilization of all four wheels. By implementing this approach, the desired tire forces and moments can be generated, which ultimately leads to improved vehicle handling and stability.

### 3.5. Tire Longitudinal Force Closed-Loop Control

To mitigate the limitations imposed on the four motors by physical conditions and ground adhesion, an optimal torque distribution control approach is employed to ensure that the upper controller’s control signal and the lower actuator’s executive signal are in agreement, effectively reducing the control level distribution error. Neglecting the dynamic characteristics of the tire in previous studies can negatively impact trajectory tracking and maneuvering performance. Thus, it is essential to control the vehicle tire force to follow the target tire force. However, measuring and controlling tire force in practice is challenging. Therefore, the sliding rate is controlled to achieve the anticipated tire force. The Dugoff tire model is employed to convert the longitudinal force to the corresponding slip rate of the tire. The Dugoff tire model is a precise model that describes the nonlinear tire characteristics and requires fewer parameters than the magic tire model, making it well-suited to inverse analysis. In this study, the Dugoff tire model is selected as the derivation model of the reverse tire model.

The Dugoff tire model can be expressed as [38]:

$$\begin{cases} F_{xi} = C_i \frac{S_i}{1+S_i} f(H_{Di}) \\ F_{yi} = k_i \frac{\tan \alpha_i}{1+S_i} f(H_{Di}) \end{cases} \quad (46)$$

where  $F_{xi}$  is the longitudinal force generated by all four hub motors;  $F_{yi}$  represents the lateral force exerted by the tires of all four wheels;  $\alpha_i$  is the lateral deflection angle of all four wheels;  $k_i$  is the lateral stiffness of the four tires;  $C_i$  is the longitudinal tire stiffness of the four wheels;  $H_{Di}$  is the tire dynamic parameter of four wheels.

$$f(H_{Di}) = \begin{cases} (2 - H_{Di})H_{Di} & H_{Di} < 1 \\ 1 & H_{Di} \geq 1 \end{cases} \tag{47}$$

where  $H_{Di} = \frac{\mu F_{zi}}{2\sqrt{(F_{xi})^2 + (F_{yi})^2}} f(H_{Di})$ .

Then,  $H_{Di} \geq 1$ ,  $f(H_{Di}) = 1$ . The longitudinal slip rate can be obtained as follows:

$$S_i = \frac{F_{xi}}{C_i - F_{xi}} \tag{48}$$

Then,  $H_{Di} < 1$ ,  $f(H_{Di}) = (2 - H_{Di})H_{Di}$ . The longitudinal sliding ratio can be obtained as follows:

$$S_i = \frac{\mu^2 F_{zi}^2 F_{xi}}{4C_i \sqrt{(F_{xi})^2 + (F_{yi})^2} \left( \mu F_{zi} - \sqrt{(F_{xi})^2 + (F_{yi})^2} \right) - \mu^2 F_{zi}^2 F_{xi}} \tag{49}$$

According to the optimal torque  $F_{xid}$  distribution of the target tire force of each wheel, the target sliding rate of the wheel can be obtained by combining the above formula:

$$F_{xid} = \frac{T_{id}}{r} \tag{50}$$

$$S_{id} = \begin{cases} \frac{F_{xid}}{C_i - F_{xid}} & H_{Di} \geq 1 \\ \frac{\mu^2 F_{zi}^2 F_{xid}}{4C_{si} \sqrt{(F_{xid})^2 + (F_{yi})^2} \left( \mu F_{zi} - \sqrt{(F_{xid})^2 + (F_{yi})^2} \right) - \mu^2 F_{zi}^2 F_{xid}} & H_{Di} < 1 \end{cases} \tag{51}$$

According to a large number of experiments, the optimal slip rate is usually in the range of 15–20%. The threshold of wheel slip rate for vehicle stability is set at 20%. If the wheel slip rate of the vehicle is 20%, the current vehicle is judged to be in a stable state, and the vehicle steady slip rate control based on the reverse tire model will be carried out. On the contrary, when 20% is determined, the vehicle is judged to be in an unstable state, making the maximum threshold of vehicle slip tracking slip rate 20%, and the ideal sliding power of the vehicle is tracked and controlled within this range.

In order to realize the longitudinal force control of vehicle, the slip rate of four wheels of vehicle is controlled indirectly. The PID control system is simple in design and high in calculation efficiency. Consequently, the PID control is used to control wheel sliding rate:

$$m(t) = K_p e(t) + K_i \int_0^t e(t) dt \tag{52}$$

where  $e(t) = S_{id} - S_i$  is the error between the expected sliding rate and the actual sliding rate of a single wheel, and  $m(t) = T_{id\_new}$  is the driving torque of a single wheel.

#### 4. Simulation

To validate the feasibility of the proposed trajectory tracking, longitudinal velocity tracking, yaw moment control layer, and tire longitudinal force control methods, we carried out simulation tests and present the results in Tables 1–3. The key parameters of the model are detailed below.

**Table 1.** Magic tire model fitting parameters.

$a_0$	$a_1$	$a_2$	$a_3$	$a_4$	$a_5$	$a_6$	$a_7$	$a_8$
1.65	−21.3	1144	49.6	226	0.069	−0.006	0.056	0.486
$b_0$	$b_1$	$b_2$	$b_3$	$b_4$	$b_5$	$b_6$	$b_7$	$b_8$
1.3	−22.1	1011	1078	1.82	0.208	0	−0.354	0.707

**Table 2.** Control parameters.

Symbol	Quantity	Value
$T$	sampling period	0.02
$N_p$	predictive time domain	20/10
$N_c$	control time domain	10/1
$K$	sliding mode switching gain	2.5
$D$		2
$\eta$		0.5
$\phi$	boundary layer thickness	0.07

**Table 3.** Vehicle parameters.

Symbol	Quantity	Value
$m$	vehicle mass	1250 kg
$h$	height of center of mass	0.54 m
$l_f$	the distance from the center of mass to the front axis	1.04 m
$l_r$	the distance from the center of mass to the rear axis	1.56 m
$I_z$	the moment of inertia of the vehicle about the z axis	1343.1 kg · m <sup>2</sup>
$d_f$	front-wheel half-pitch	0.74 m
$d_r$	rear-wheel half-pitch	0.7425 m
$r$	effective rolling radius of wheel	0.298 m
$k_f$	front-wheel lateral stiffness	75,875 N · rad <sup>−1</sup>
$k_r$	rear-wheel side stiffness	75,875 N · rad <sup>−1</sup>
$C_f$	longitudinal stiffness of front wheel	161,145 N
$C_r$	longitudinal stiffness of rear wheel	161,145 N

To enhance the credibility of the suggested control algorithm for trajectory tracking, we carried out a simulation verification while varying the speed of the vehicle and the coefficient of friction between the tires and the ground. This additional analysis aimed to determine the effectiveness of the control algorithm under different conditions.

- (1) To further confirm the effectiveness of the trajectory tracking control algorithm, a simulation study was carried out by varying the vehicle speed and the ground adhesion coefficient. The vehicle speeds of 60 km/h, 50 km/h, and 30 km/h were considered, with a fixed ground adhesion coefficient of 0.85. The main focus was on the vehicle's trajectory tracking and stability when following a double line-shifting trajectory. Figure 4 presents the simulation results.

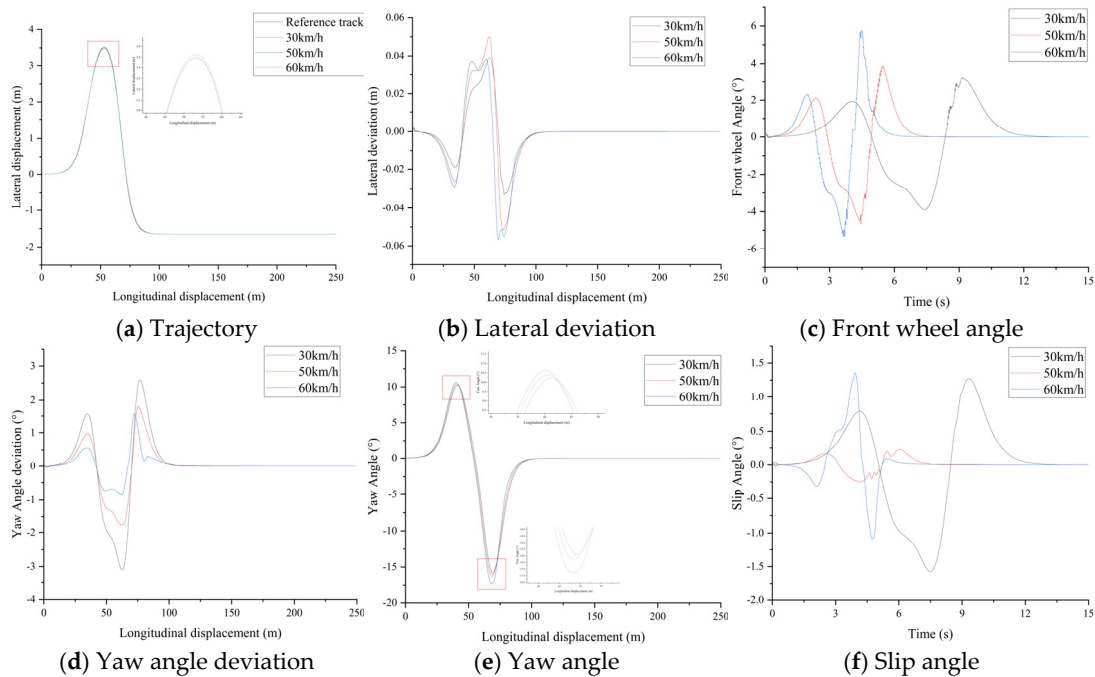


**Figure 4.** Simulation results of control system trajectory tracking under different velocity variations.

The simulation results in Figure 4 demonstrate the effectiveness of the proposed vehicle trajectory tracking and stability control strategy at different speeds. The deviation in lateral displacement of the vehicle, as illustrated in Figure 4b,c, rises as the speed increases, but remains within a consistent range. The steering angle of the front wheel also grows with the speed. Additionally, as seen in Figure 4d–f, the yaw angle of the vehicle increases in proportion to the speed, while the lateral inclination angle of the center of mass remains relatively stable. These findings demonstrate the precision and dependability of the suggested control algorithm for path tracking in the face of varying vehicle speeds and ground adhesion coefficients.

- (2) To further validate the effectiveness of the proposed trajectory tracking control algorithm, simulations were conducted with variations in ground adhesion coefficient and vehicle speed. Specifically, the vehicle speed was set to 35 km/h, while the ground adhesion coefficients were set to 0.85, 0.5, and 0.25. The performance of the vehicle trajectory tracking and stability control was evaluated under the condition of a double-shift track. The simulation results are illustrated in Figure 5.

To confirm the efficiency of the suggested control algorithm in following the intended path, simulations were conducted using varying ground adhesion coefficients and vehicle speeds. The results of the simulations, depicted in Figure 5a, demonstrate the validity of the proposed method for vehicle trajectory tracking and stability control strategy, which is accurate and effective under differing adhesion coefficients. Further analysis from Figure 5b,c indicates that the lateral displacement error of the vehicle remains stable under high adhesion, but significantly increases on low-adhesion ground. Additionally, the front wheel angle remains relatively constant across different adhesion coefficients. The simulation results (Figure 5d–f) demonstrate that the vehicle’s yaw angle increases with decreasing adhesion coefficient, and the centroid’s lateral declination angle fluctuates when the adhesion coefficient is as low as 0.25. However, the lateral declination angle of the centroid is largely unaffected by changes in the adhesion coefficient under high adhesion conditions. These findings suggest that the proposed control algorithm is robust and capable of maintaining stability and accuracy in trajectory tracking under varying conditions.

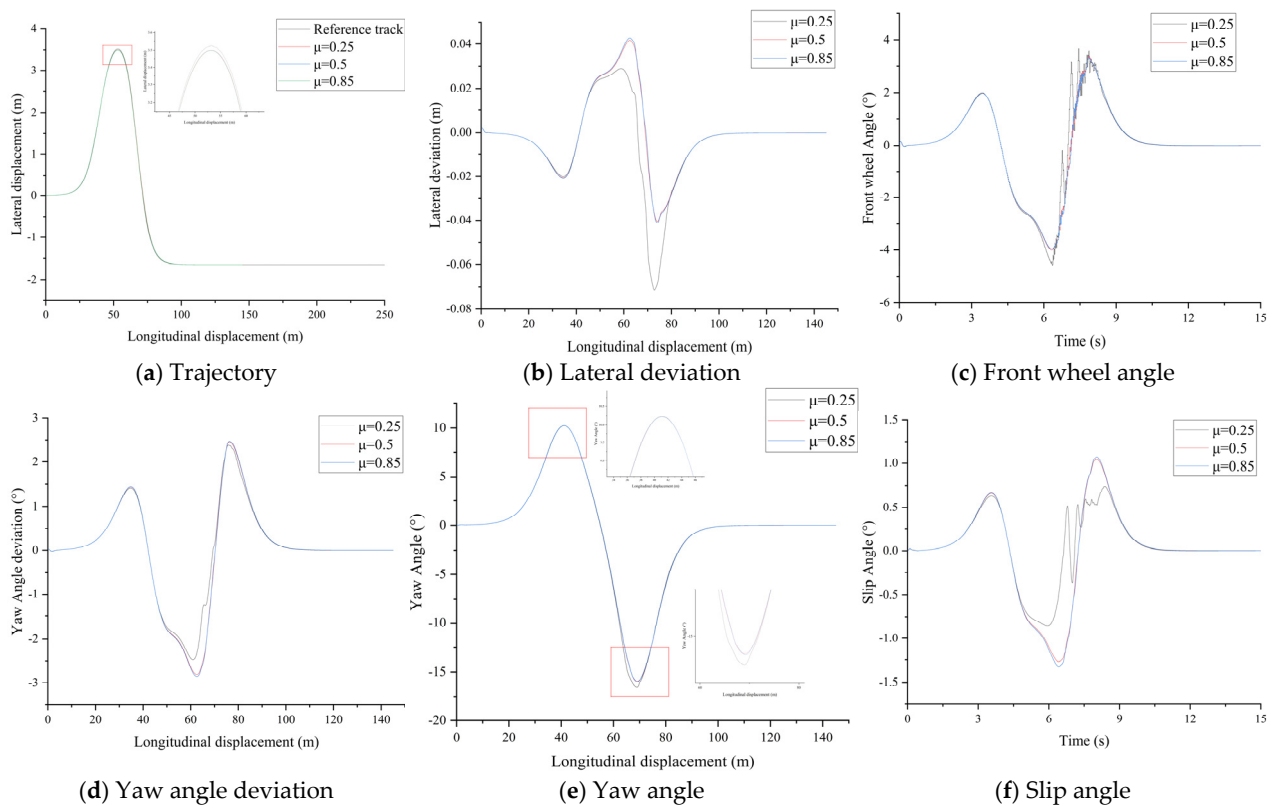


**Figure 5.** Simulation results of control system trajectory tracking under different adhesion coefficient variations.

To further demonstrate the efficacy of the proposed control strategy, simulation tests were conducted to evaluate its performance under double-shift and single-shift conditions with a large road curvature. The double-shift condition, which involves emergency avoidance or steering situations, and the single-shift condition, which mimics actual lane changes, were chosen for their representativeness. The simulation utilized the vehicle's front-wheel steering system and employed an independently driving torque distribution.

For standard vehicles, the adhesion coefficient plays a crucial role in the tire's grip on the road. Lower adhesion coefficients make it challenging to meet the necessary steering requirements during medium- and high-speed driving, ultimately leading to unstable driving conditions. Thus, this study aims to investigate the effects of vehicle speed and ground adhesion coefficient on the double-shift line working condition. The simulation conditions for this study were set as follows: (1) the vehicle's velocity remains unchanged at 60 km/h and the ground adhesion coefficient remains constant at 0.85, and (2) the vehicle speed is constant at 50 km/h and the adhesion coefficient is constant at 0.5. The simulation results are illustrated in Figures 6 and 7.

This study introduces a novel multi-closed-loop control principle that prioritizes tire longitudinal force control and aims to achieve a shorter control response time. To enable the closed-loop control of tire longitudinal force, control is transformed into tire longitudinal sliding rate control via the tire inverse model. To demonstrate the effectiveness and superiority of the proposed multi-closed-loop control, this study compares the simulation results of general control (no slip-rate control) and integrated control with the multi-closed-loop control algorithm proposed herein. The simulation conditions that were chosen included a double-shift condition with a large curvature, representative of emergency avoidance or steering. Figure 6 displays the outcomes for a constant adhesion coefficient of 0.85 on the ground and a steady vehicle velocity of 60 km/h.

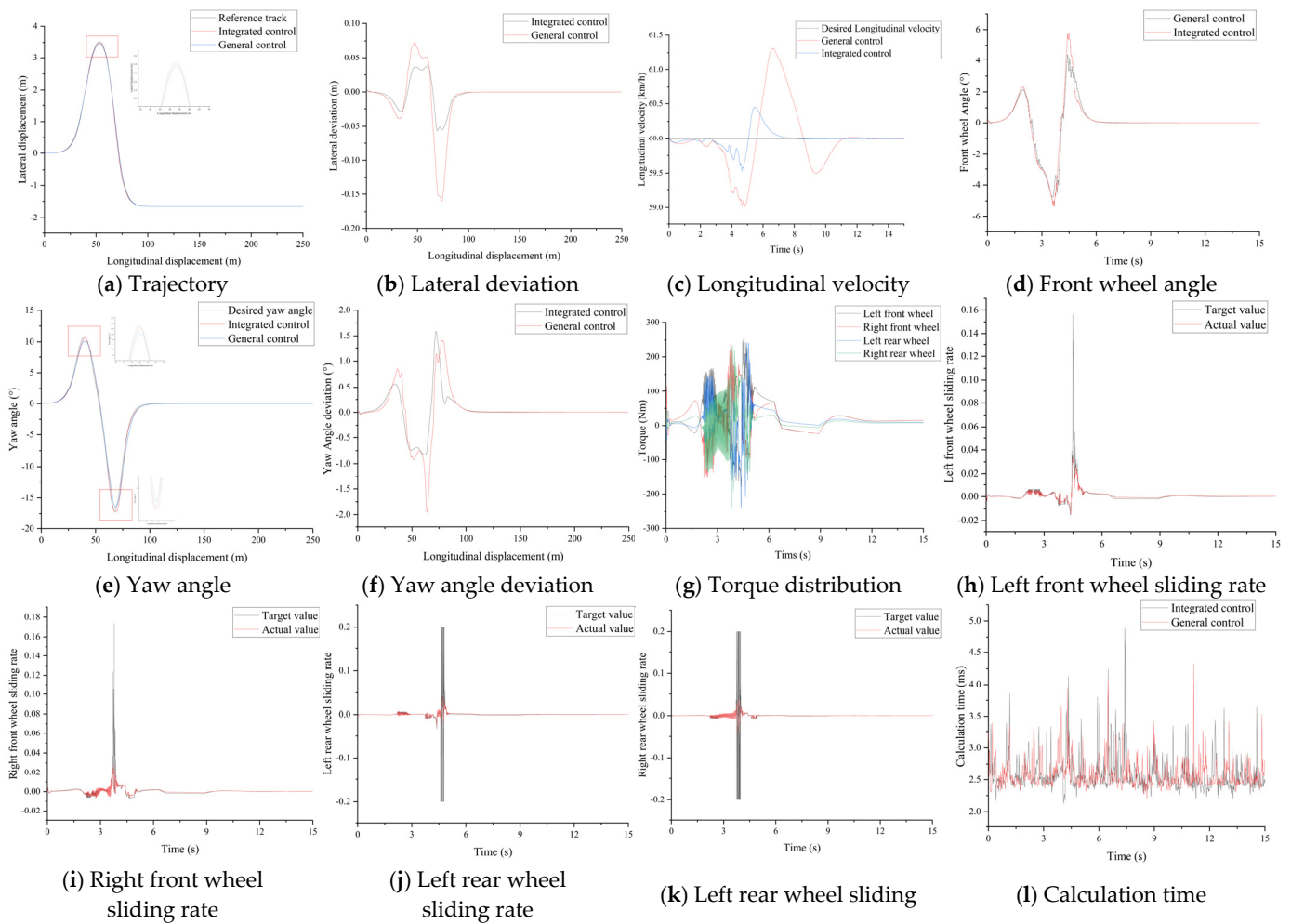


**Figure 6.** Simulation results of the two control algorithms at a ground adhesion coefficient of 0.85 and vehicle speed of 60 km/h.

From the results presented in Figure 6a,b, it is clear that the proposed control strategy is more effective and accurate in tracking the trajectory in comparison to the general control strategy. The multi-closed-loop control proposed in this paper reduces the lateral error by 55.6% in comparison to the general control strategy. Additionally, in Figure 6c–f, it can be observed that the multi-closed-loop control has better speed and front wheel angle tracking, with minimal fluctuations in speed and front wheel angle. The transverse sway angle tracking is also effective with a smaller error, thereby avoiding vehicle instability. Figure 6g–k demonstrate that the vehicle is better distributed among the four wheels under the optimal torque distribution and tire longitudinal force integrated control. The actual sliding rate of the four wheels aligns with the target values, improving the maneuvering stability during trajectory tracking. Finally, Figure 6l compares the calculation time, with an average calculation time of 2.57 ms for the proposed algorithm and 2.58 ms for the general control. The comparison shows that the proposed algorithm has a shorter control response time and higher response speed.

To evaluate the vehicle’s ability to maintain stability and follow a desired trajectory in low-adhesion environments and at moderate speeds, a double-shift line test was conducted on the vehicle. The simulation outcomes for a vehicle velocity of 50 km/h and a ground adhesion coefficient of 0.5 are illustrated below.

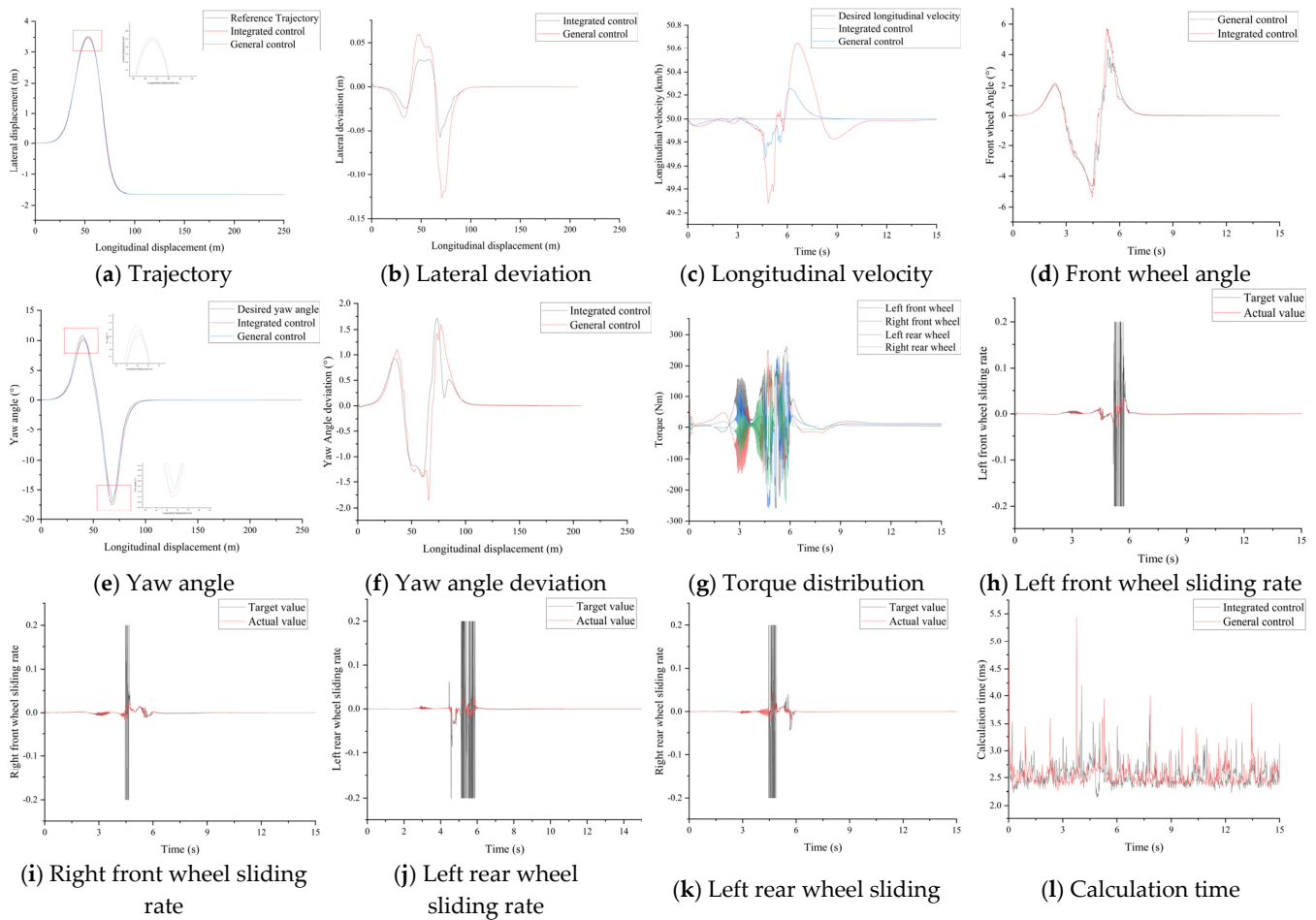


**Figure 7.** Simulation results of the two control algorithms at a ground adhesion coefficient of 0.5 and vehicle speed of 50 km/h.

To evaluate the vehicle’s trajectory tracking and maneuvering stability at medium speeds under low adhesion conditions, we conducted a double-shift line condition test. Figure 7 depicts the simulation results at a ground adhesion coefficient of 0.5 and a vehicle speed of 50 km/h, which demonstrate the practicability of the proposed multi-closed-loop integrated control strategy under these conditions. According to the simulation results at a ground adhesion coefficient of 0.5 and a vehicle speed of 50 km/h, the proposed control strategy exhibits a superior performance compared to the general control strategy in maintaining trajectory accuracy and reducing dynamic fluctuations in speed and front wheel corner tracking. The cross-swing angle also shows less error and fluctuates near the desired value, thereby avoiding vehicle instability during trajectory tracking. Furthermore, the proposed integrated control strategy’s response time is 2.53 ms, which is faster than the general control time of 2.55 ms, indicating a more rapid response time for the integrated control system.

To assess the efficiency of the proposed integrated control algorithm under low-adhesion conditions and high speed, a single line-shifting test was carried out by setting the vehicle speed at a constant 100 km/h and the ground adhesion coefficient at 0.5. The simulation findings of the vehicle’s yaw stability and trajectory tracking are presented in Figure 8.

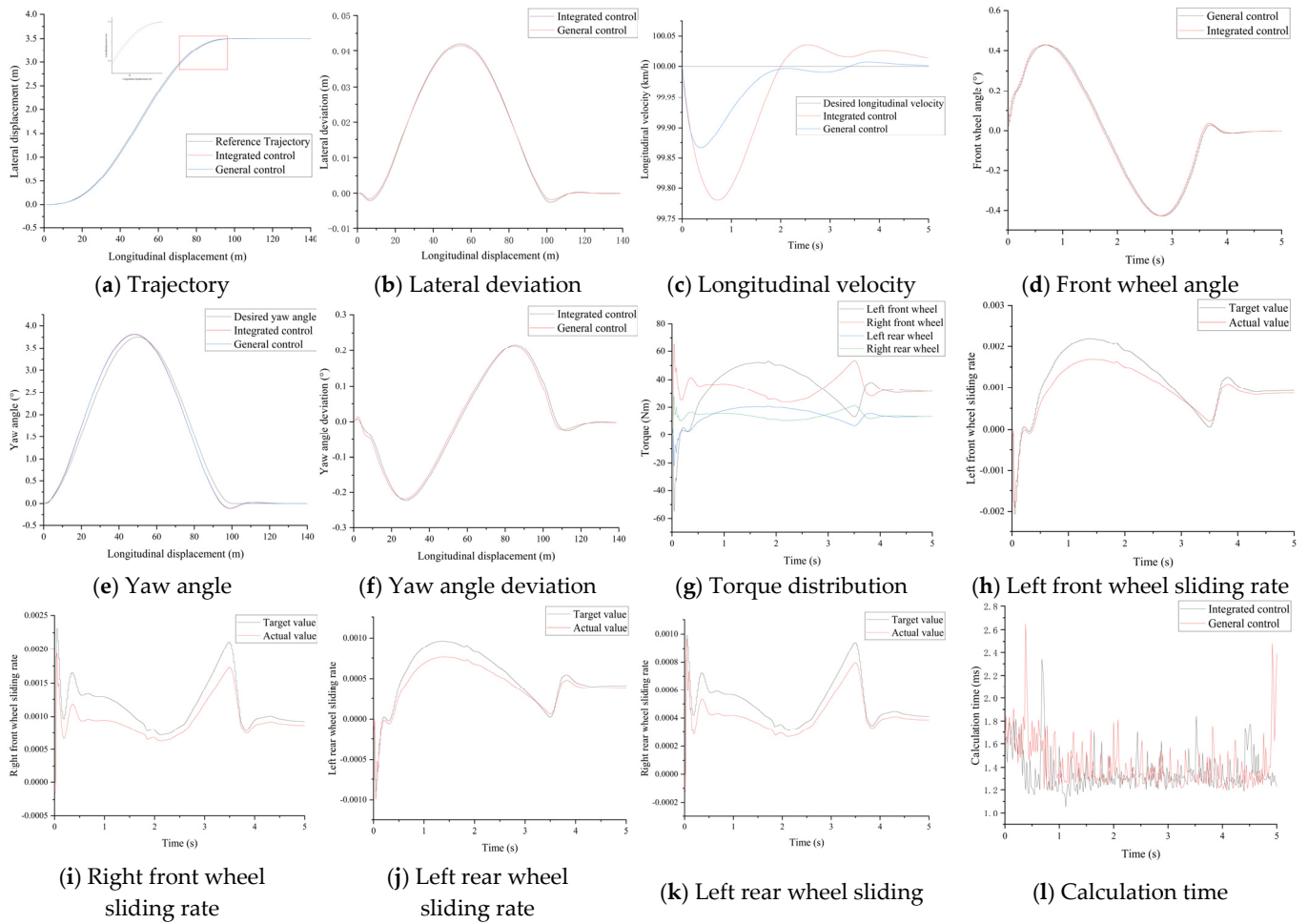


**Figure 8.** Simulation results of the two control algorithms at a ground adhesion coefficient of 0.5 and vehicle speed of 100 km/h.

The effectiveness of the integrated control algorithm proposed in this paper is demonstrated by the results of the single line-shifting test conducted at a constant speed of 100 km/h and a ground adhesion coefficient of 0.5. The simulation results presented in Figure 8 show that the proposed algorithm performs well in terms of trajectory tracking and yaw stability, even under challenging high-speed and low-adhesion conditions. The lateral error is significantly reduced in comparison to the general control approach. Both the integrated and general control algorithms (no slip rate control) exhibit good performance in vehicle speed tracking, with the general control (no slip rate control) approach exhibiting slightly less fluctuation. No significant difference is observed in the front wheel angle under the two control algorithms. Furthermore, both approaches effectively control vehicle stability during trajectory tracking. The tire sliding rate graphic of the integrated control shows that the actual sliding rate of the wheel tracks the target value well during vehicle operation, resulting in a better distribution of driving torque among the vehicle wheels. The results indicate that the proposed integrated control algorithm outperforms the general control strategy in terms of response time by 0.07 ms. This suggests that the algorithm has the potential to enhance vehicle safety and performance in challenging driving scenarios.

**5. Conclusions**

The integrated control of vehicle trajectory tracking and yaw stability is achieved in this paper through the utilization of multiple control algorithms. This paper validates the effectiveness of our proposed integrated control algorithm, where we build a co-simulation platform of MATLAB/Simulink and CarSim. The simulation results demonstrate the

algorithm's applicability under different vehicle speeds and ground adhesion coefficients. In terms of trajectory tracking, the vehicle can track the trajectory well under control, and the deviation error is small. In terms of vehicle stability, the vehicle ensured stability under control, in line with the expected results. We further verified the algorithm's performance under different working conditions, including a high vehicle speed and high ground adhesion coefficient, a low ground adhesion coefficient at medium vehicle speed, and a low ground adhesion coefficient at high vehicle speed, with double and single line shifts. A comparison with general control (no slip rate control) shows that our multi-closed-loop integrated control algorithm is more advanced in terms of trajectory tracking and yaw stability control, with a shorter computational response time.

In this paper, an intelligent vehicle dynamic model driven by a four-wheel hub motor is established. Based on the intelligent vehicle dynamic model, the advantages of distributed drive are fully utilized. The intelligent vehicle dynamics model and tire force closed-loop (slip rate control) method can further improve vehicle trajectory tracking performance and driving stability, and provide a research basis and theoretical basis for future researchers to further study intelligent vehicle trajectory tracking and yaw stability integrated control. The MPC, SMC and PID control algorithms used in this paper are practical and can be reliably applied to real vehicles. The simulation method can reduce the cost of intelligent vehicle development. The integrated control of trajectory tracking and yaw stability will be widely used in intelligent vehicles in the future, further promoting the development of intelligent vehicles and safe and reliable direction.

**Author Contributions:** Conceptualization, J.L. (Jing Li); writing—original draft, J.L. (Jin Luo); writing—review and editing, S.G.; supervision, B.F. All authors have read and agreed to the published version of the manuscript.

**Funding:** This work was supported by the National Key Research and Development Program (Project number: 2018YFB010590502).

**Data Availability Statement:** The data are listed in the article.

**Conflicts of Interest:** The authors declare no conflicts of interest.

## References

1. Elbanhawi, M.; Simic, M.; Jazar, R. Receding Horizon Lateral Vehicle Control for Pure Pursuit Path Tracking. *J. Vib. Control* **2018**, *24*, 619–642. [[CrossRef](#)]
2. Ohta, H.; Akai, N.; Takeuchi, E.; Kato, S. Pure Pursuit Revisited: Field Testing of Autonomous Vehicles in Urban Areas. In Proceedings of the IEEE 4th international Conference on Cyber-Physical Systems, Networks, and Applications (CPSNA), Nagoya, Japan, 6–7 October 2016; pp. 7–12.
3. Ziegler, J.; Bender, P.; Schreiber, M.; Lategahn, H.; Strauß, T.; Stiller, C.; Dang, T.; Franke, U.; Appenrodt, N.; Keller, C.G.; et al. Making bertha drive—an autonomous journey on a historic route. *IEEE Intell. Transp. Syst. Mag.* **2014**, *6*, 8–20. [[CrossRef](#)]
4. Macadam, C.C. Application of an optimal preview control for simulation of closed-loop automobile driving. *IEEE Trans. Syst. Man Cybern.* **2007**, *11*, 393–399. [[CrossRef](#)]
5. Guo, K.; Fancher, P.S. Preview-follower method for modeling closed-loop vehicle directional control. In Proceedings of the 19th Annual Conference on Manual Control, Cambridge, MA, USA, 23–25 May 1983.
6. Wei, X.; Li, J.; Liu, X. LQR Control Scheme for Active Vehicle Suspension Systems Based on Modal Decomposition. In Proceedings of the 25th Chinese Control and Decision Conference (CCDC), Guiyang, China, 25–27 May 2013; pp. 3296–3301.
7. Riofrio, A.; Sanz, S.; Boada MJ, L.; Boada, B.L. A LQR-Based Controller with Estimation of Road Bank for Improving Vehicle Lateral and Rollover Stability Via Active Suspension. *Sensors* **2017**, *17*, 2318. [[CrossRef](#)] [[PubMed](#)]
8. Cheng, S.; Li, L.; Chen, X.; Wu, J.; Wang, H.D. Model Predictive Control Based Path Tracking Controller of Autonomous Vehicle Considering Parametric Uncertainties and Velocity Varying. *IEEE Trans. Ind. Electron.* **2021**, *68*, 8698–8707. [[CrossRef](#)]
9. Choi, Y.; Lee, W.; Kim, J.; Yoo, J. A Variable-Sampling Time Model Predictive Control Algorithm for Improving Path-Tracking Performance of a Vehicle. *Sensors* **2021**, *21*, 6845. [[CrossRef](#)]
10. Shen, C.; Shi, Y.; Buckham, B. Trajectory Tracking Control of an Autonomous Underwater Vehicle Using Lyapunov-Based Model Predictive Control. *IEEE Trans. Industrial Electron.* **2018**, *65*, 5796–5805. [[CrossRef](#)]
11. Wang, H.; Liu, B.; Ping, X.; Quan, A. Path tracking control for autonomous vehicles based on an improved MPC. *IEEE Access.* **2019**, *7*, 161064–161073. [[CrossRef](#)]

12. Sun, C.; Zhang, X.; Zhou, Q.; Tian, Y. A model predictive controller with switched tracking error for autonomous vehicle path tracking. *IEEE Access*. **2019**, *7*, 53103–53114. [[CrossRef](#)]
13. Bai, G.; Meng, Y.; Liu, L.; Luo, W.; Gu, Q.; Li, K. A New Path Tracking Method Based on Multilayer Model Predictive Control. *Appl. Sci.* **2019**, *9*, 2649. [[CrossRef](#)]
14. Wu, H.; Si, Z.; Li, Z. Trajectory Tracking Control for Four-Wheel Independent Drive Intelligent Vehicle Based on Model Predictive Control. *IEEE Access*. **2020**, *8*, 73071–73081. [[CrossRef](#)]
15. Zhang, Z.Y.; Long, K.; Du, R.; Huang, C. Trajectory tracking coordinated control for autonomous vehicle in high-speed overtaking. *Auton. Eng.* **2021**, *43*, 995–1004.
16. Kabzan, J.; Hewing, L.; Linger, A.; Zeilinger, M. Learning based model predictive control for autonomous racing. *IEEE Robot. Autom. Lett.* **2019**, *3363*, 3363–3370. [[CrossRef](#)]
17. Rosolia, U.; Zhang, X.; Borrelli, F. Data-driven predictive control for autonomous systems. *Annu. Rev. Control. Robotics Auton. Syst.* **2018**, *1*, 259–286. [[CrossRef](#)]
18. Leman, Z.A.; Ariff, M.H.M.; Zamzuri, H.; Rahman, M.A.A.; Mazlan, S.A. Model predictive controller for path tracking and obstacle avoidance manoeuvre on autonomous vehicle. In Proceedings of the 12th Asian Control Conference (ASCC), Kitakyushu, Japan, 9–12 June 2019; pp. 1271–1276.
19. Tian, Y.; Yao, Q.; Wang, C.; Wang, S.; Liu, J. Switched model predictive controller for path tracking of autonomous vehicle considering rollover stability. *Veh. Syst. Dyn.* **2022**, *60*, 4166–4185. [[CrossRef](#)]
20. Hashemi, E.; Qin, Y.; Khajepour, A. Slip-aware driver assistance path tracking and stability control. *Control. Eng. Pract.* **2022**, *118*, 104958. [[CrossRef](#)]
21. Toropov, E.; Tumasov, A.; Vashurin, A.; Butin, D.; Stepanov, E. Hardware-in-the-Loop Testing of Vehicle's Electronic Stability Control System. *Appl. Eng. Lett. J. Eng. Appl. Sci.* **2023**, *8*, 70–79. [[CrossRef](#)]
22. Ren, Y.; Zhang, L.; Khajepour, A. Integrated model predictive and torque vectoring control for path tracking 4-wheel-driven autonomous vehicles. *IET Intell. Transp. Syst.* **2019**, *13*, 98–107. [[CrossRef](#)]
23. Ataei, M.; Khajepour, A.; Jeon, S. Model predictive control for integrated lateral stability, traction/braking control, and rollover prevention of electric vehicles. *Veh. Syst. Dyn.* **2020**, *58*, 49–73. [[CrossRef](#)]
24. Chen, L.; Xie, Y.P.; Cai, Y.F.; Sun, X.Q.; Teng, C.L.; Zou, K. Stable tracking control of autonomous vehicles at extreme conditions. *Automot. Eng.* **2020**, *42*, 1016–1026.
25. Ryosuke, E.; Kazuomi, S.; Junya, Y. Driving force distribution based on tyre energy for independent wheel-drive vehicle on rough ground. *J. Terramechanics* **2018**, *76*, 29–38.
26. Mokhiamar, O.; Abe, M. Simultaneous optimal distribution of lateral and longitudinal tire forces for the model following control. *J. Dyn. Syst. Meas. Control* **2004**, *126*, 753–763. [[CrossRef](#)]
27. Novellis, L.D.; Sornioti, A.; Patrick, G. Wheel torque distribution criteria for electric vehicles with torque-vectoring differentials. *IEEE Trans. Veh. Technol.* **2014**, *63*, 1593–1602. [[CrossRef](#)]
28. Zhang, Z.; Xie, L.; Lu, S.; Wu, X.; Su, H. Vehicle yaw stability control with a two-layered learning MPC. *Veh. Syst. Dyn.* **2023**, *63*, 423–444. [[CrossRef](#)]
29. Lin, F.; Qian, C.; Cai, Y.; Zhao, Y.; Wang, S.; Zang, L. Integrated tire slip energy dissipation and lateral stability control of distributed drive electric vehicle with mechanical elastic wheel. *J. Frankl. Inst.* **2022**, *359*, 4776–4803. [[CrossRef](#)]
30. Zhai, L.; Wang, C.; Houand, Y.; Liu, C. MPC-Based Integrated Control of Trajectory Tracking and Handling Stability for Intelligent Driving Vehicle Driven by Four Hub Motor. *IEEE Trans. Veh. Technol.* **2022**, *71*, 2668–2680. [[CrossRef](#)]
31. Hans, P. *Tyre and Vehicle Dynamics*; Butterworth-Heinemann: Oxford, UK, 2002.
32. Shaobo, L.U. *Study on Vehicle Chassis Key Subsystems and Its Integrated Control Strategy*; Chongqing University: Chongqing, China, 2009.
33. Zhang, L.; Wang, Z.; Sun, F.; Wang, Z. Research on Steering Failure Tolerance Control of Intelligent Electric Vehicle Driven by Four-wheel hub Motor. *Chin. J. Mech. Eng.* **2021**, *57*, 141–152.
34. Gong, J.; Liu, K.; Qi, J. *Autonomous Vehicle Model Predictive Control*; Beijing Institute of Technology Press: Beijing, China, 2020.
35. Yu, Z. *Automobile Theory*, 5th ed.; China Beijing Machine Press: Beijing, China, 2009.
36. Liu, J. *Sliding Mode Variable Structure Control MATLAB Simulation 4th edition—Basic Theory and Design Method*; Tsinghua University Press: Beijing, China, 2019.
37. Wang, F. *Research on Motion Control of Distributed Intelligent Electric Vehicles under Extreme Working Conditions*; Dalian University of Technology: Dalian, China, 2021.
38. Nenggen, D.; Saied, T. A Modified Dugoff Tire Model for Combined-slip Forces. *Tire Sci. Technol.* **2010**, *38*, 228–244.

**Disclaimer/Publisher's Note:** The statements, opinions and data contained in all publications are solely those of the individual author(s) and contributor(s) and not of MDPI and/or the editor(s). MDPI and/or the editor(s) disclaim responsibility for any injury to people or property resulting from any ideas, methods, instructions or products referred to in the content.